Jet quenching in the glasma stage of heavy-ion collisions

HP2024
NAGASAKI

Andrey Sadofyev
LIP, Lisbon

LABORATÓRIO DE INSTRUMENTAÇÃO
E FÍSICA EXPERIMENTAL DE PARTÍCULAS

Heavy-ion collisions

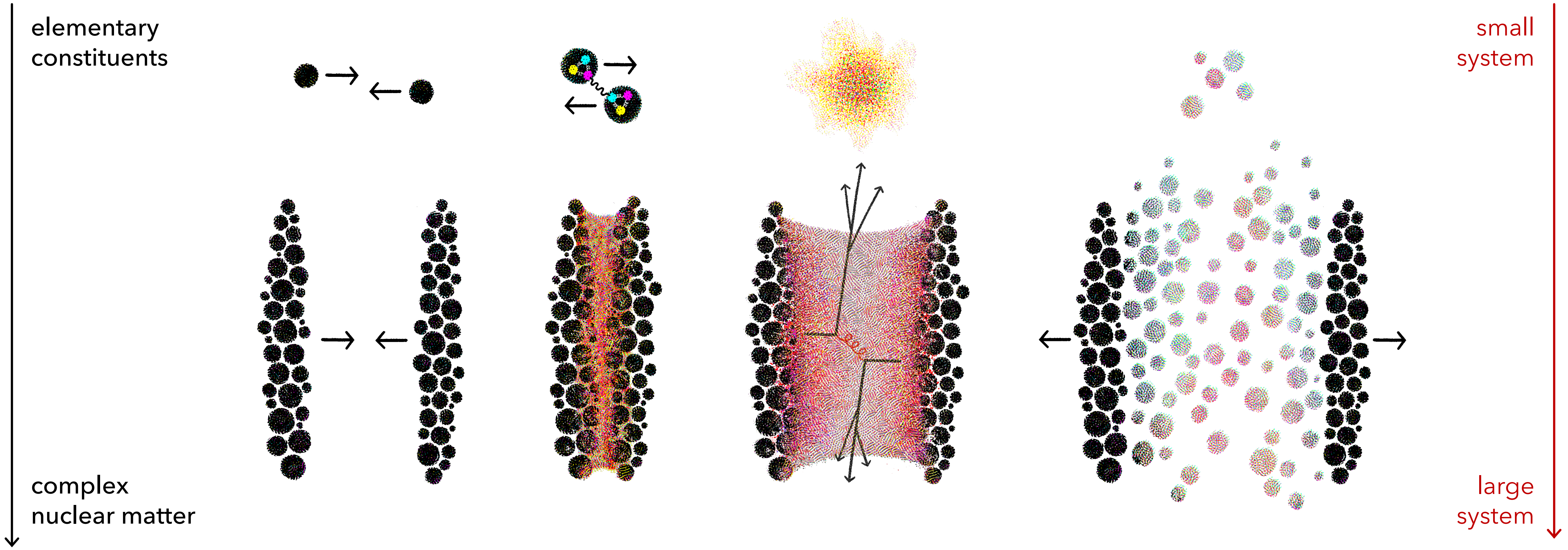

Jet tomography

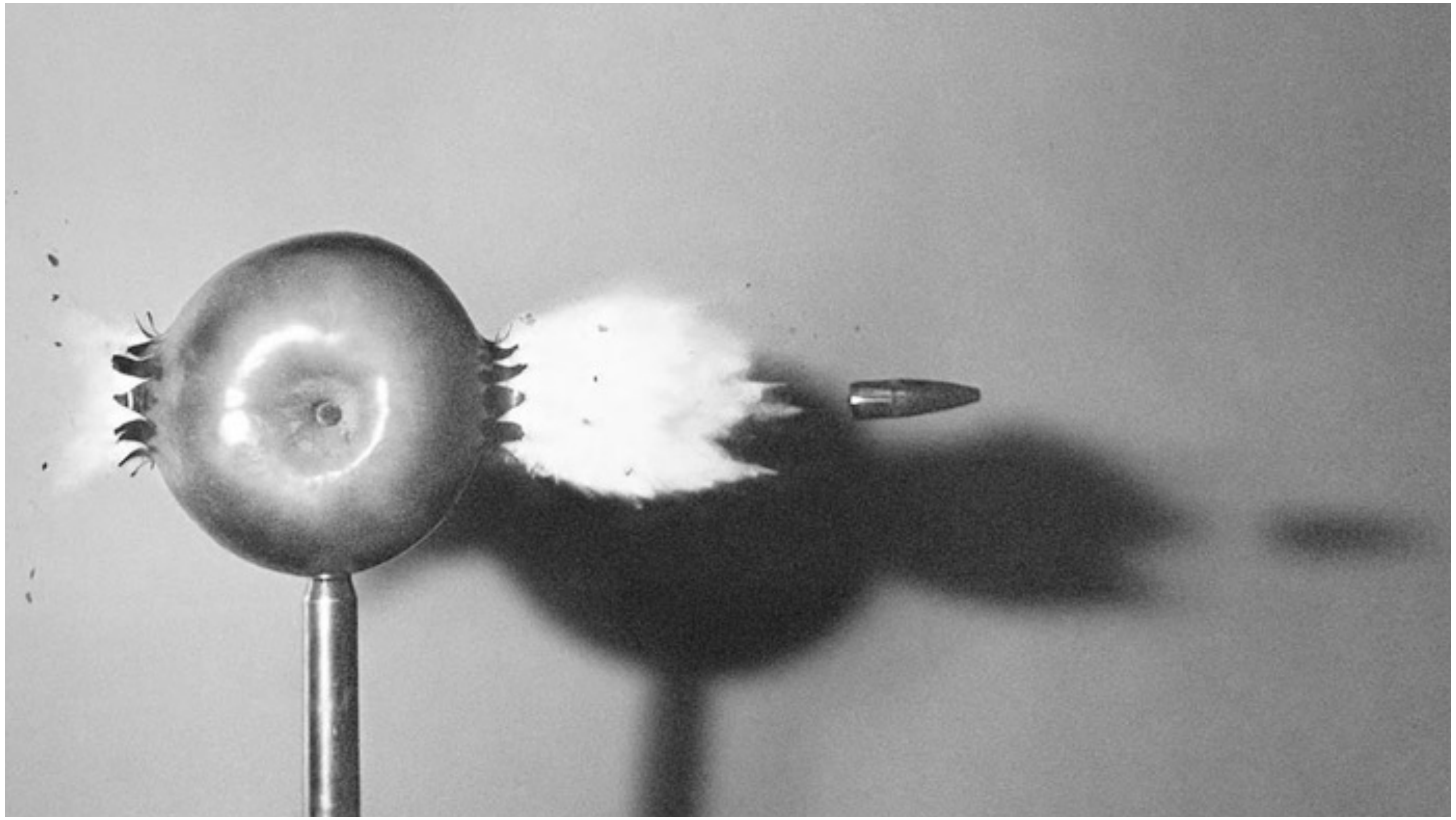

Jet tomography

AS, M. Sievert, I. Vitev, PRD, 2021
J. Barata, AS, C. Salgado, PRD, 2022
C. Andres, F. Dominguez, AS, C. Salgado, PRD, 2022
J. Barata, AS, X.-N. Wang, PRD, 2023
J. Barata, X. Mayo, AS, C. Salgado, PRD, 2023
M. Kuzmin, X. Mayo, J. Reiten, AS, PRD, 2024
J. Barata, G. Milhano, AS, EPJC, 2024

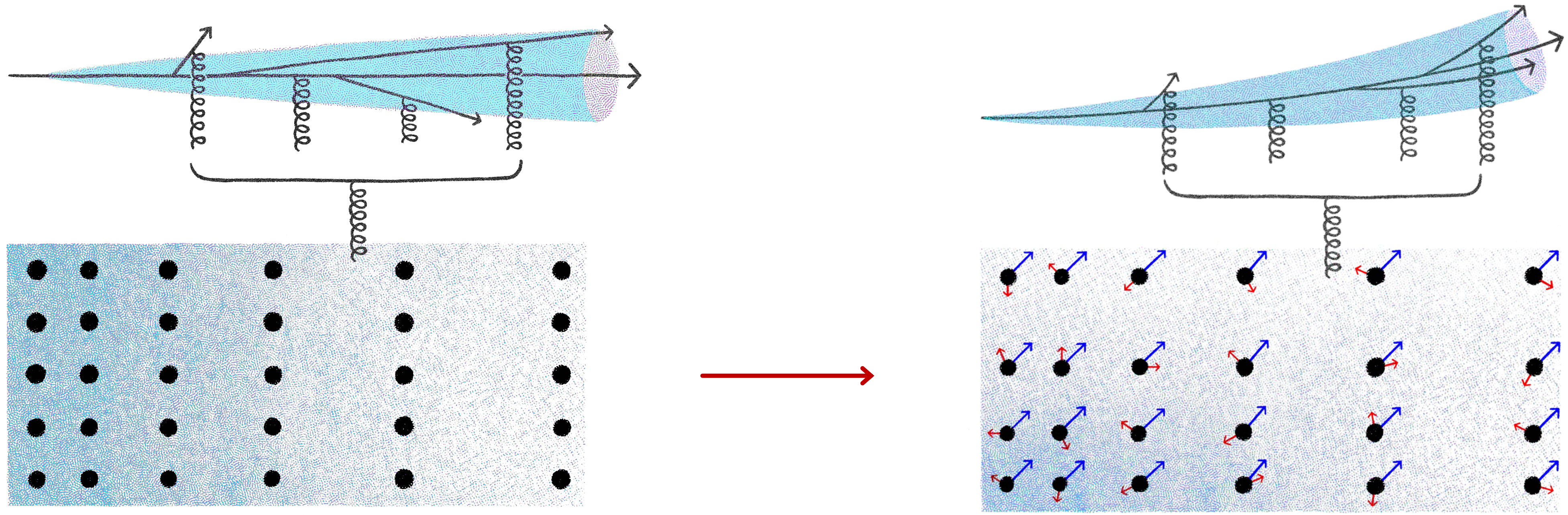

see the talks by J. Bahder (Tue), T. Luo (Wed), R. Fries (Wed), X. Mayo (Wed), C. Salgado (Wed), J. Silva (Wed)

Jet tomography

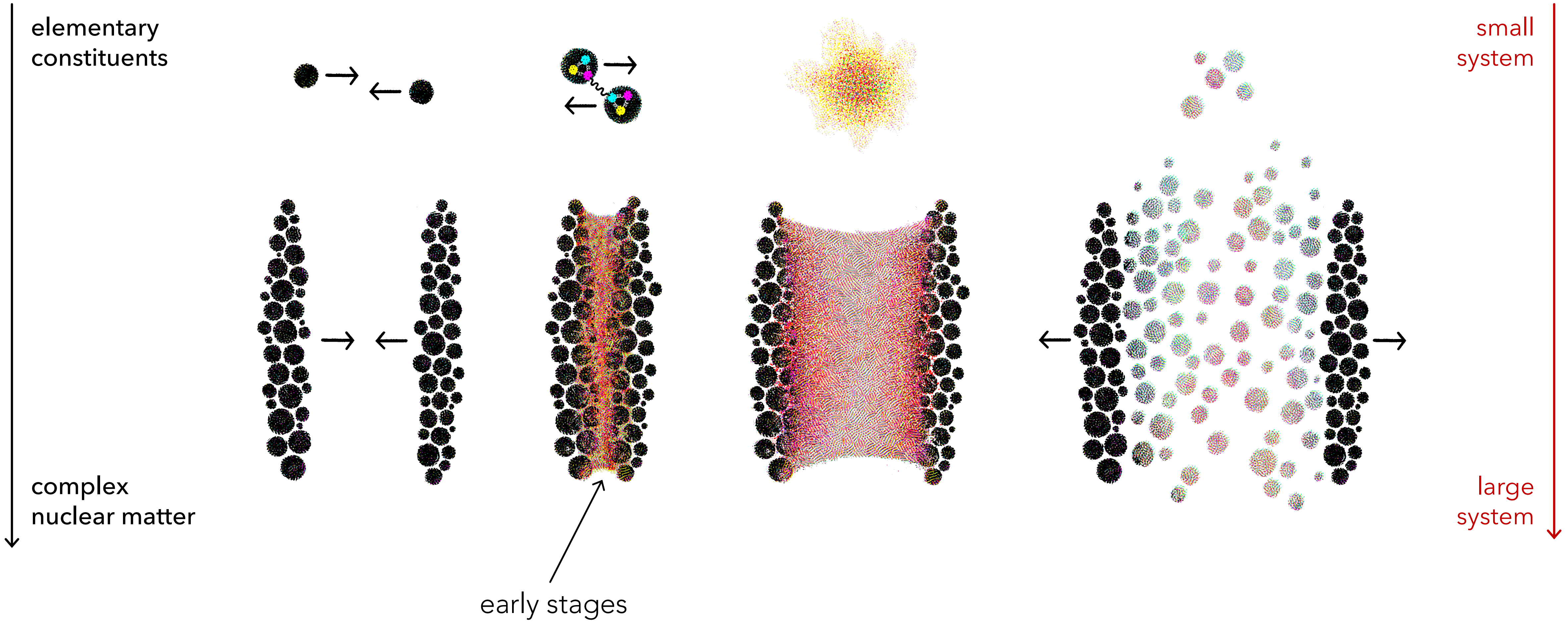

M. E. Carrington, A. Czajka, S. Mrowczynski, NPA, 2020
A. Ipp, D. I. Müller, D. Schuh, PRD, 2020
A. Ipp, D. I. Müller, D. Schuh, PLB, 2020
M. E. Carrington, A. Czajka, S. Mrowczynski, PLB, 2022
M. E. Carrington, A. Czajka, S. Mrowczynski, PRC, 2022
D. Avramescu et al., PRD, 2023

Momentum broadening in glasma

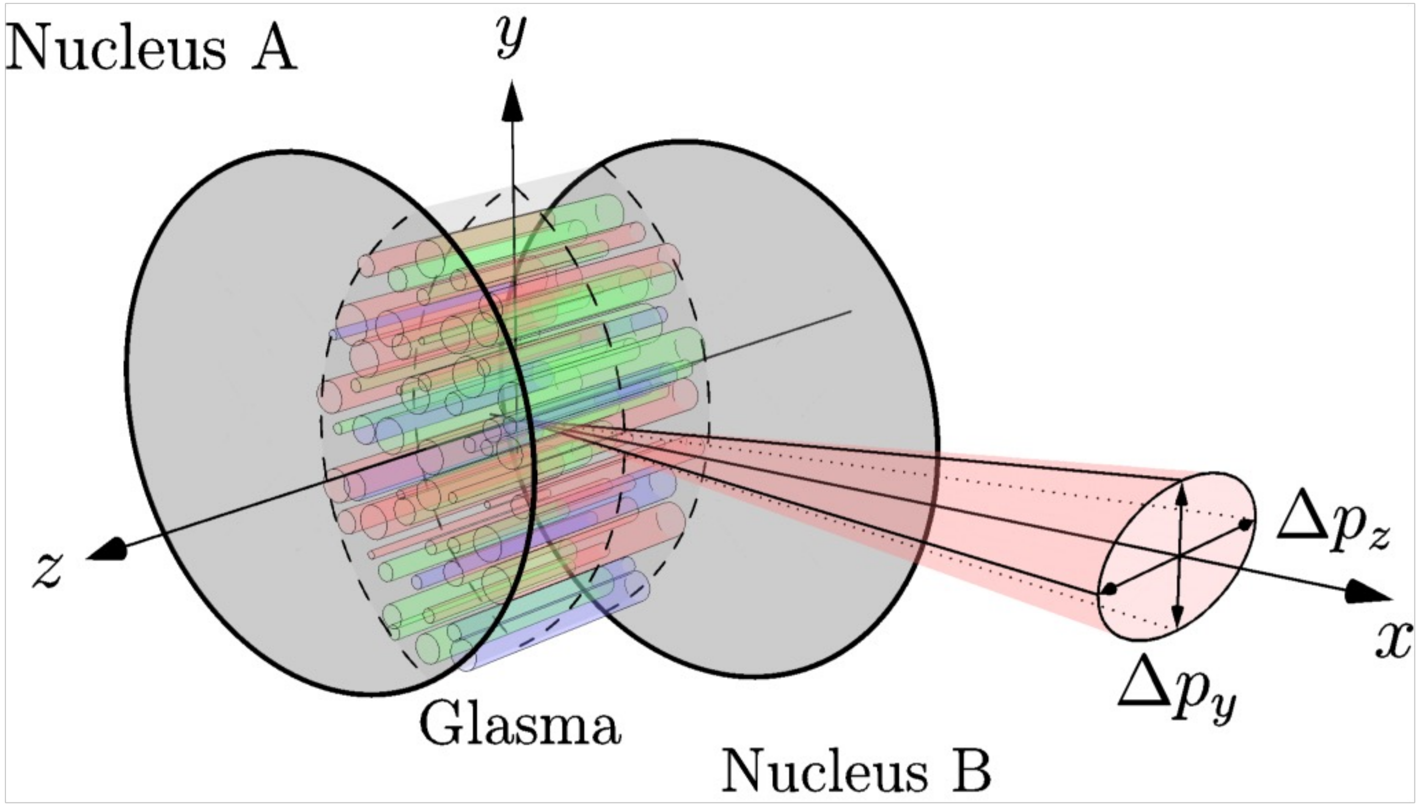

*M. E. Carrington, A. Czajka, S. Mrowczynski, NPA, 2020
A. Ipp, D. I. Müller, D. Schuh, PRD, 2020
A. Ipp, D. I. Müller, D. Schuh, PLB, 2020
M. E. Carrington, A. Czajka, S. Mrowczynski, PLB, 2022
M. E. Carrington, A. Czajka, S. Mrowczynski, PRC, 2022
D. Avramescu et al., PRD, 2023
**K. Boguslavski et al., PLB, 2024
K. Boguslavski et al., PRD, 2024

Momentum broadening in glasma

- $\hat{q}$ is hard to access experimentally, but it provides an important measure for phenomenological estimates;
- Simulations, see e.g. JETSCAPE (PRC, 2021), suggest that a typical value for the QGP at $\mathbf{T = 200\ MeV}$ is $\mathbf{\hat{q} = 0.12\ GeV^2/fm}$;
- The glasma phase was assumed less relevant, but the recent works* indicate that $\mathbf{\hat{q} \geq 5\ GeV^2/fm}$ during the first $\mathbf{0.3\ fm/c}$;
- Moreover, the simulations of the non-equilibrium dynamics within kinetic theory** show **continuity of $\hat{q}$** consistent with these glasma phase values;

see the talks by F. Lindenbauer (Mon), S. Barrera (Mon), C. Lamas (Mon), D. Avramescu (Tue)

Energy loss

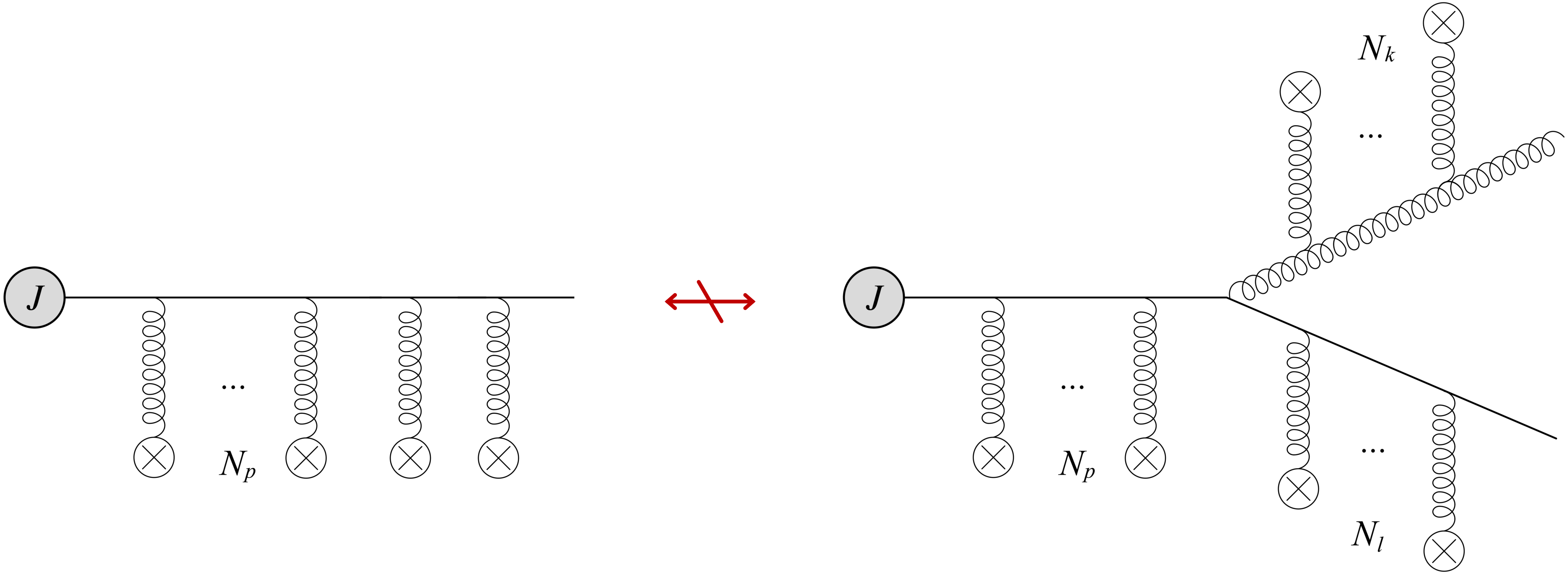

energy loss is not solely defined by $\hat{q}$

Color potential

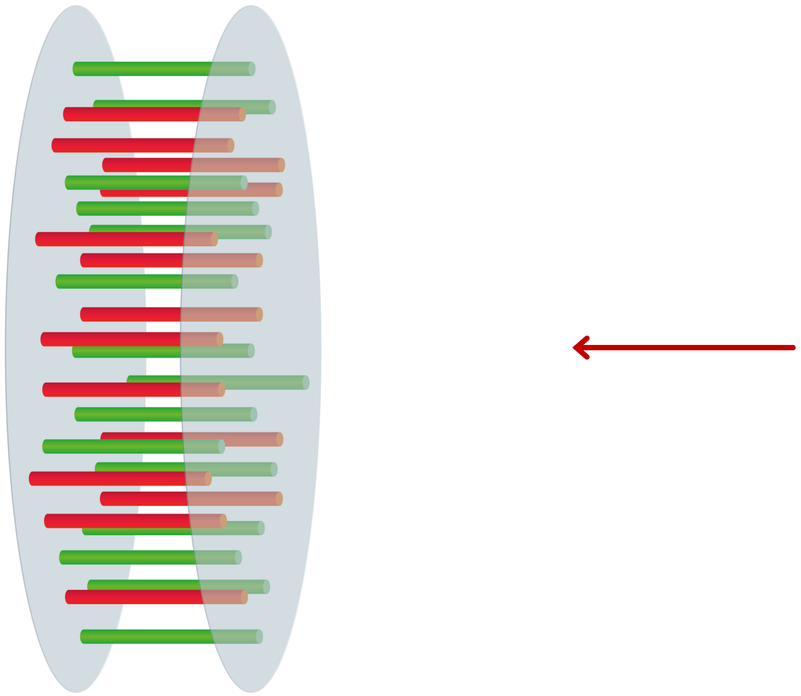

David Müller, thesis (arxiv), 2019

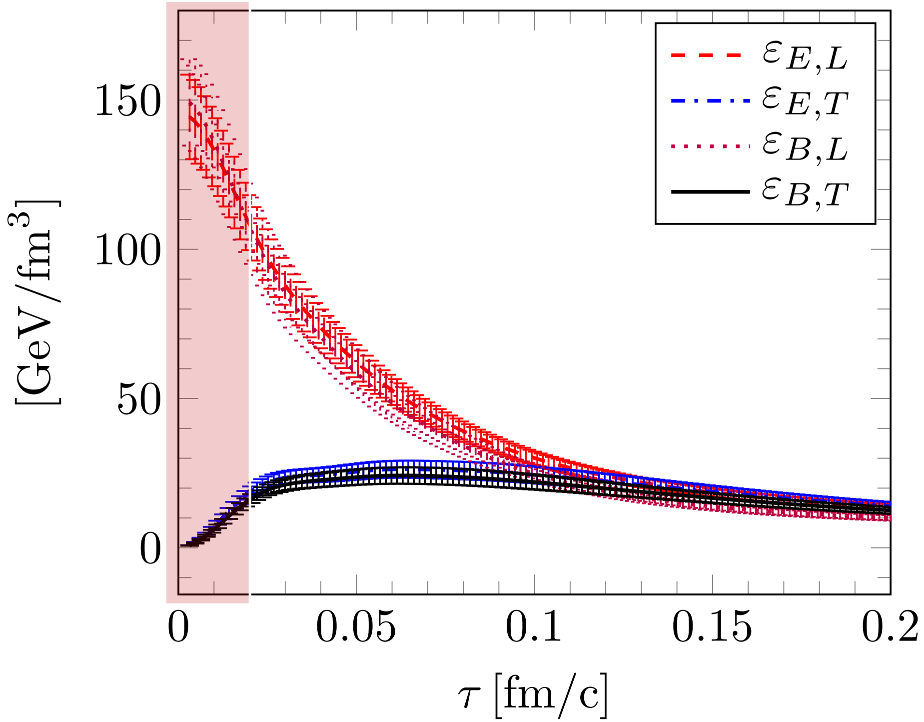

Color potential

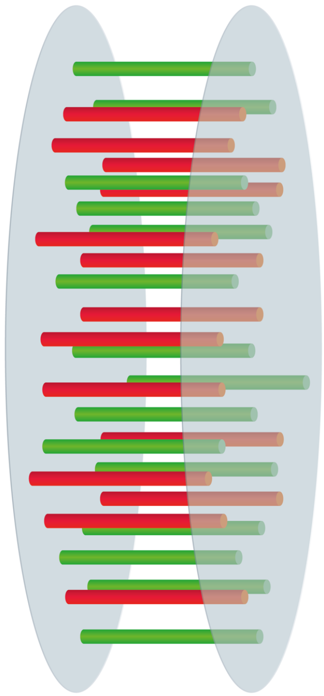

tube size ↓

$$A^{a\mu}_{\rm coh} = \begin{cases} \delta^{\mu 0}\mathbf{x}\cdot\mathbf{E}^a_1, & 0 \le z < \ell \\ \delta^{\mu 0}\mathbf{x}\cdot\mathbf{E}^a_2, & \ell \le z < 2\ell \\ \delta^{\mu 0}\mathbf{x}\cdot\mathbf{E}^a_3, & 2\ell \le z < 3\ell \\ \vdots \end{cases}$$

$$\langle \ldots \rangle = \prod_i \int_{E_{ix}} e^{-E_{ix}^2/E_0^2} \ldots$$

Broadening (BDMPS-Z style)

$$\hat{q} = -\frac{1}{2(2\pi)^3\mathcal{N}}\frac{\partial}{\partial L}\int_{\mathbf{x}} \boldsymbol{\nabla}^2_{\mathbf{x}-\bar{\mathbf{x}}}\Big(J^\dagger(\bar{\mathbf{x}})\mathcal{W}^\dagger(\bar{\mathbf{x}})\mathcal{W}(\mathbf{x})J(\mathbf{x})\Big)_{\bar{\mathbf{x}}=\mathbf{x}}$$

Broadening (BDMPS-Z style)

$$\hat{q} = -\frac{1}{2(2\pi)^3\mathcal{N}} \frac{\partial}{\partial L} \int_{\mathbf{x}} \boldsymbol{\nabla}^2_{\mathbf{x}-\bar{\mathbf{x}}} \Big(J^\dagger(\bar{\mathbf{x}}) \mathcal{W}^\dagger(\bar{\mathbf{x}}) \mathcal{W}(\mathbf{x}) J(\mathbf{x}) \Big)_{\bar{\mathbf{x}}=\mathbf{x}}$$

$\downarrow$

the width of the initial distribution

$$\hat{q}(z) = \frac{w^2}{2\pi^3} \int_{\mathbf{Y}} \int_0^z d\bar{\tau}\, \tilde{\mathcal{W}}^{ab}(\mathbf{Y}; z, \bar{\tau})\, E^a_x(z) E^b_x(\bar{\tau}) e^{-2w^2\mathbf{Y}^2}$$

Broadening (BDMPS-Z style)

$$\hat{q} = -\frac{1}{2(2\pi)^3 \mathcal{N}} \frac{\partial}{\partial L} \int_{\mathbf{x}} \nabla^2_{\mathbf{x}-\bar{\mathbf{x}}} \Big(J^\dagger(\bar{\mathbf{x}}) \mathcal{W}^\dagger(\bar{\mathbf{x}}) \mathcal{W}(\mathbf{x}) J(\mathbf{x}) \Big)_{\bar{\mathbf{x}}=\mathbf{x}}$$

↓

the width of the initial distribution

$$\hat{q}(z) = \frac{w^2}{2\pi^3} \int_{\mathbf{Y}} \int_0^z d\bar{\tau}\, \tilde{\mathcal{W}}^{ab}(\mathbf{Y}; z, \bar{\tau})\, E^a_x(z) E^b_x(\bar{\tau}) e^{-2w^2 \mathbf{Y}^2}$$

↓

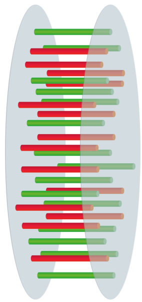

$$\langle \hat{q}(z) \rangle_{\mathrm{SU}(N_c)} = \frac{N_c^2 - 1}{8\pi^2} E_0^2(z - z_n)$$

Broadening (BDMPS-Z style)

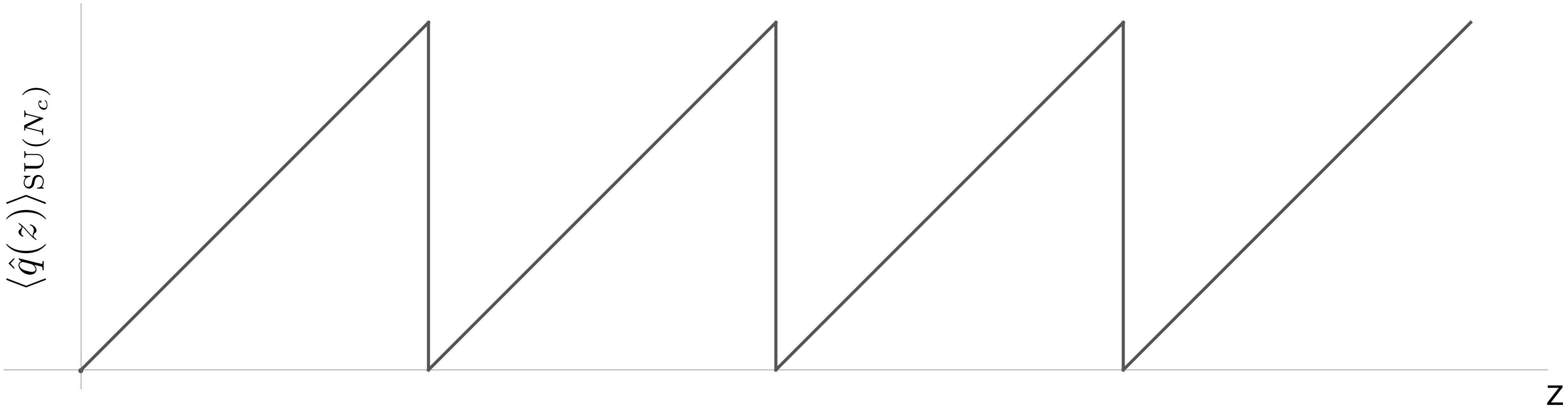

$$\langle \hat{q}(z) \rangle_{\mathrm{SU}(N_c)} = \frac{N_c^2 - 1}{8\pi^2} E_0^2 (z - z_n) \quad \longrightarrow \quad \langle \hat{q}(z) \rangle_{\mathrm{SU}(N_c), z_{in}} = \frac{N_c^2 - 1}{16\pi^2} E_0^2 \ell$$

Broadening (BDMPS-Z style)

- Within each tube parton momentum grows linearly with time/path;

- At the edge of the next tube, the interference takes over, and the process restarts;

- Averaging over the position in the first tube, we get a smoothed physical result within our model;

- And now, we also have some insight into how the gluon radiation should behave;

Gluon emission (BDMPS-Z style)

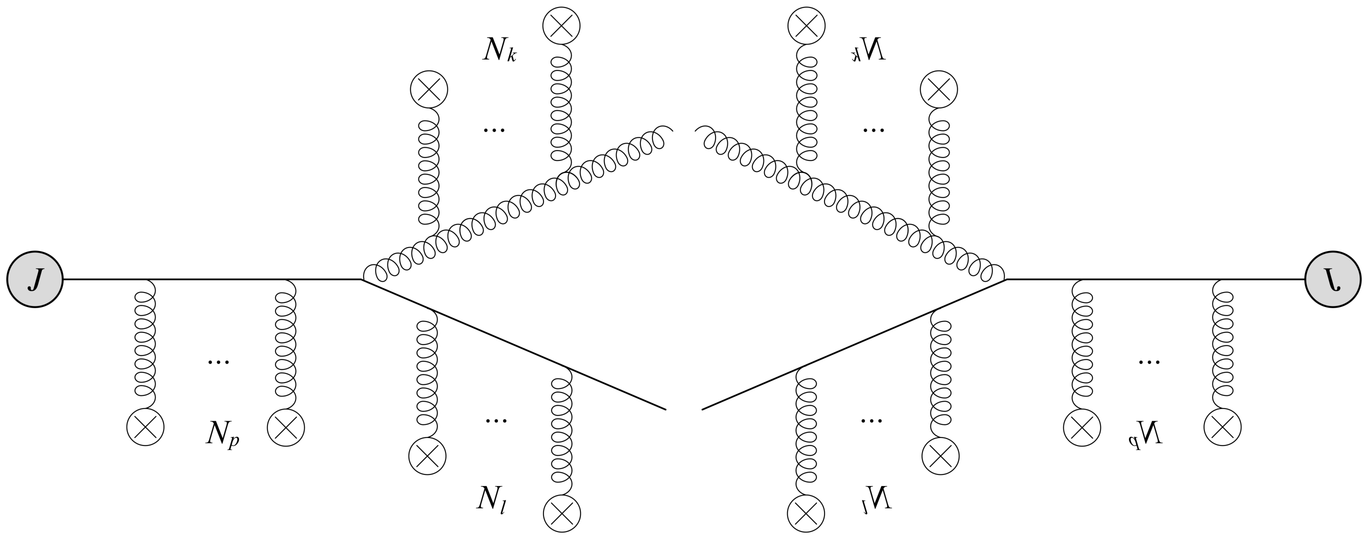

$$2(2\pi)^3\omega E\frac{d\mathcal{N}}{d\omega dEd^2\mathbf{k}} = \lim_{z_f\to\infty}\frac{\alpha_s}{N_c\,\omega^2}\,\mathrm{Re}\int_0^\infty d\bar{z}\int_0^{\bar{z}} dz\int_{\mathbf{x}_{in}}|J(\mathbf{x}_{in})|^2$$
$$\times\left\langle\left[\nabla_{\alpha,\mathbf{x}_{in}}\mathcal{G}^{ba}\left(\mathbf{k},z_f;\mathbf{x}_{in},z\right)\right]\tilde{\mathcal{W}}^{\dagger\,a\bar{a}}(\mathbf{x}_{in};\bar{z},z)\left[\nabla_{\alpha,\mathbf{x}_{in}}\mathcal{G}^{\dagger\,\bar{a}b}\left(\mathbf{k},z_f;\mathbf{x}_{in},\bar{z}\right)\right]\right\rangle\;,$$

Gluon emission (BDMPS-Z style)

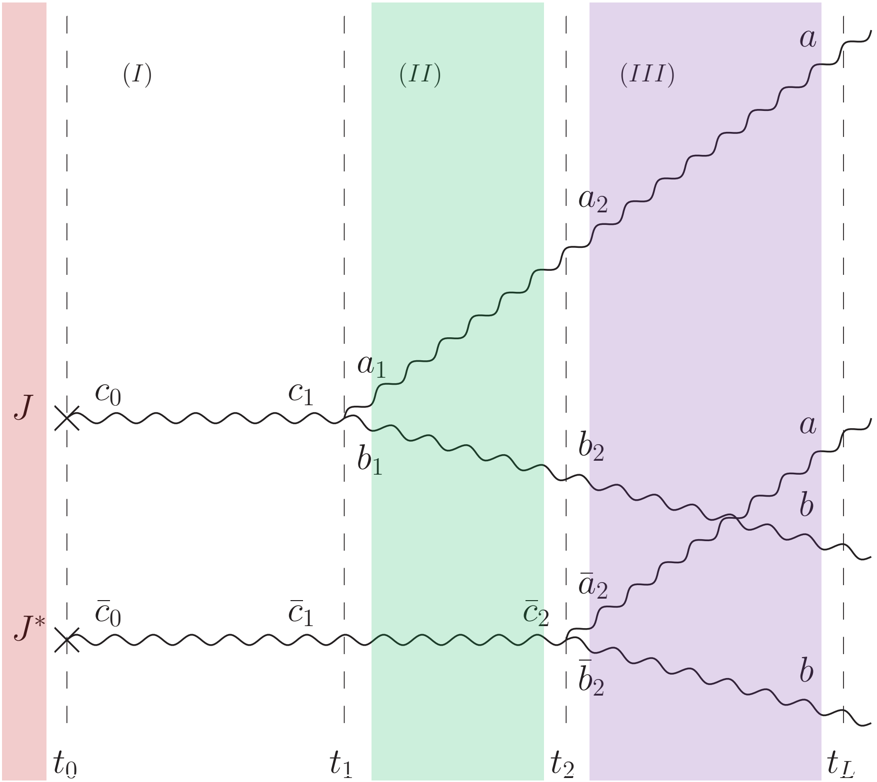

$$\left\langle t_i^a t_j^b \right\rangle = \mathcal{C}\delta_{ij}\delta^{ab}$$

$$\updownarrow$$

$$\left\langle \hat{\rho}^a(\mathbf{x}, z)\hat{\rho}^b(\bar{\mathbf{x}}, \bar{z}) \right\rangle = \frac{\rho(z)}{2C_{\bar{R}}}\delta^{ab}\,\delta^{(2)}(\mathbf{x}-\bar{\mathbf{x}})\,\delta(z-\bar{z})$$

Gluon emission (BDMPS-Z style)

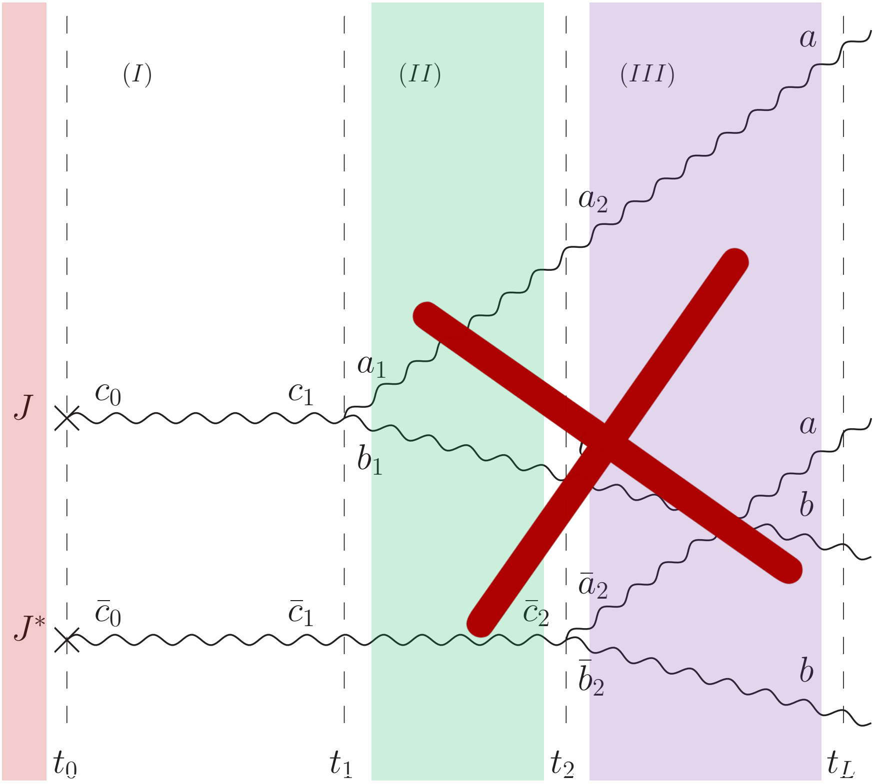

$$\left\langle t_i^a t_j^b \right\rangle = \mathcal{C}\delta_{ij}\delta^{ab}$$

$$\updownarrow$$

$$\left\langle \hat{\rho}^a(\mathbf{x}, z)\hat{\rho}^b(\bar{\mathbf{x}}, \bar{z})\right\rangle = \frac{\rho(z)}{2C_{\bar{R}}}\delta^{ab}\,\delta^{(2)}(\mathbf{x}-\bar{\mathbf{x}})\,\delta(z-\bar{z})$$

c.f.

$$A^{a\mu}_{\text{coh}} = \begin{cases} \delta^{\mu 0}\mathbf{x}\cdot\mathbf{E}^a_1, & 0 \le z < \ell \\ \delta^{\mu 0}\mathbf{x}\cdot\mathbf{E}^a_2, & \ell \le z < 2\ell \\ \delta^{\mu 0}\mathbf{x}\cdot\mathbf{E}^a_3, & 2\ell \le z < 3\ell \\ \vdots \end{cases}$$

The average cannot be factorized

Gluon emission (BDMPS-Z style)

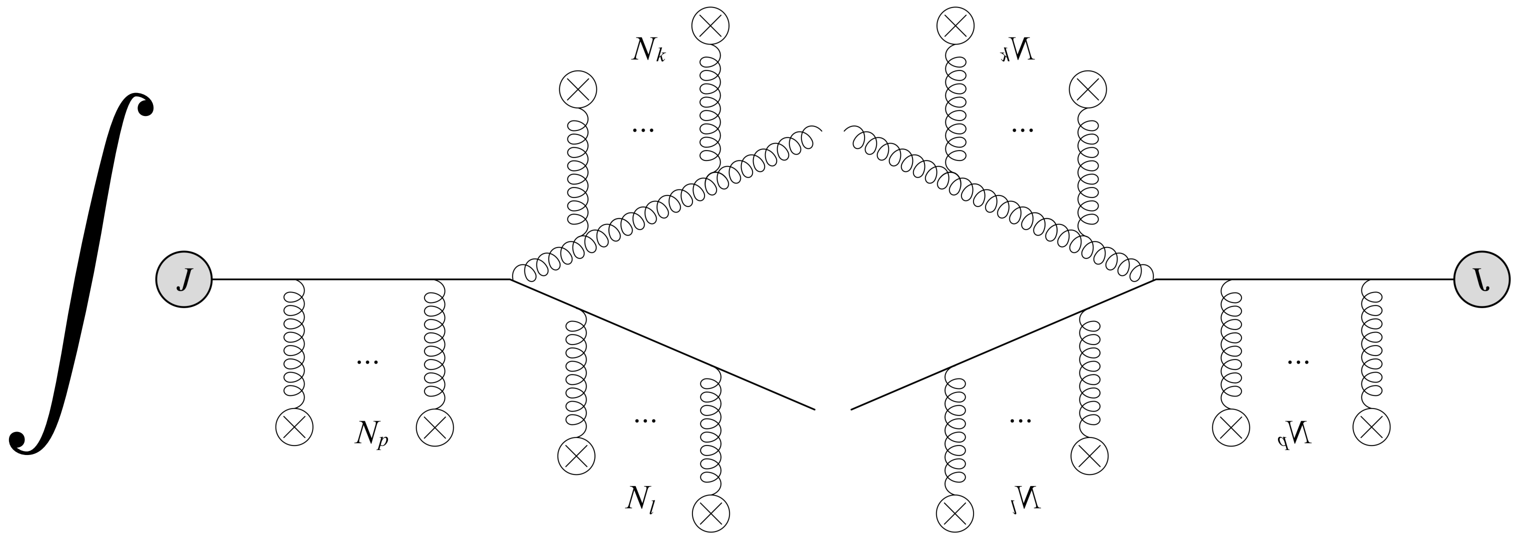

$$\frac{d\Gamma}{d\mathrm{x}} = \frac{2\alpha_s C_F}{\mathrm{x}\omega^2}\mathrm{Re}\int_0^t ds\,\boldsymbol{\nabla}_{\mathbf{x}}\cdot\boldsymbol{\nabla}_{\mathbf{y}}\Big(\mathcal{K}(\mathbf{x},t;\mathbf{y},s) - \mathcal{K}_0(\mathbf{x},t;\mathbf{y},s)\Big)_{\mathbf{x}=\mathbf{y}=0}$$

The case of U(1) fields (single tube)

$t_{\mathrm{ch}} = (24\omega/E^2)^{1/3}$

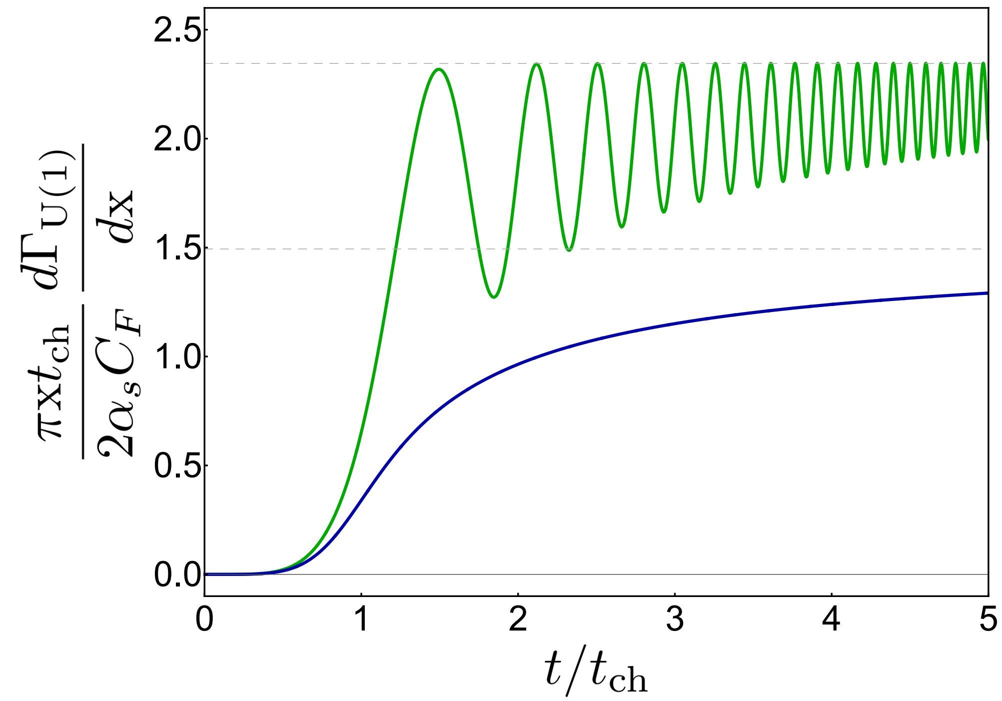

$\omega_{\mathrm{ch}} = E^2 t^3/24$

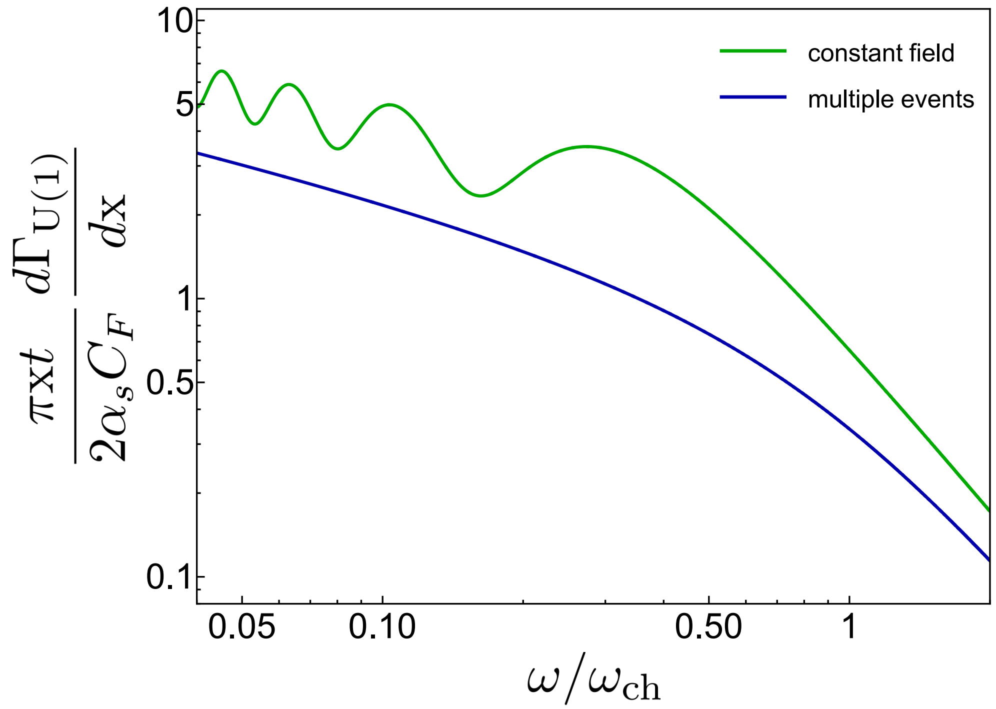

$$\frac{d\Gamma_{\mathrm{U(1)}}}{d\mathrm{x}} = \frac{2\alpha_s C_F}{\mathrm{x}\pi} \mathrm{Re} \int_0^t ds \, \frac{1}{s^2} \left(1 - \left(1 - i \frac{E^2 s^3}{8\omega} \right) e^{-i \frac{E^2 s^3}{24\omega}} \right)$$

The case of U(1) fields (single tube)

$t_{\rm ch} = (24\omega/E^2)^{1/3}$

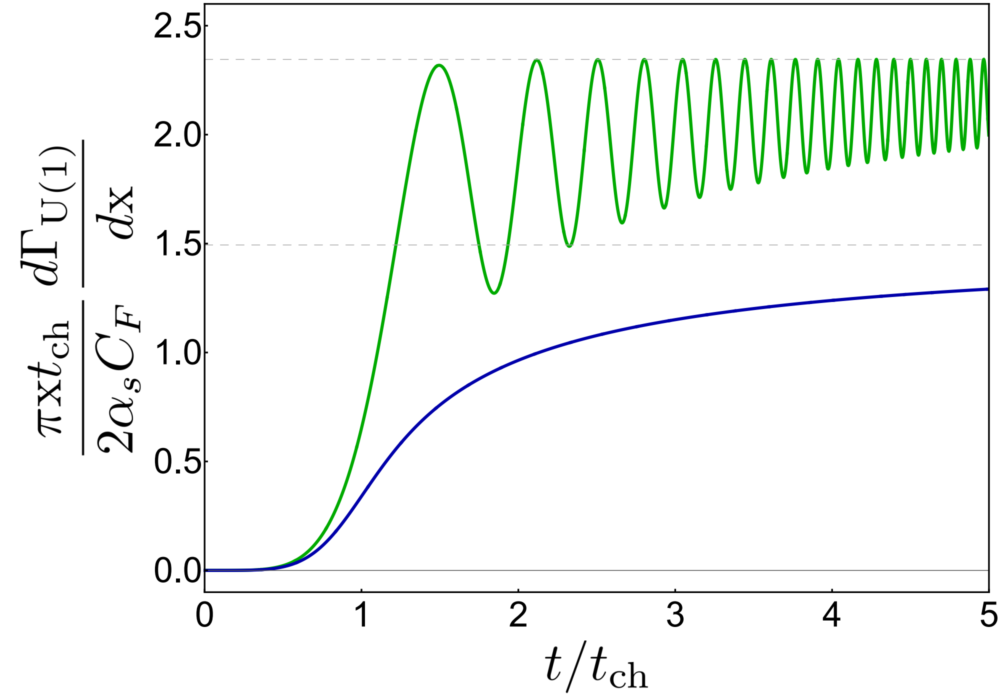

$\omega_{\rm ch} = E^2 t^3/24$

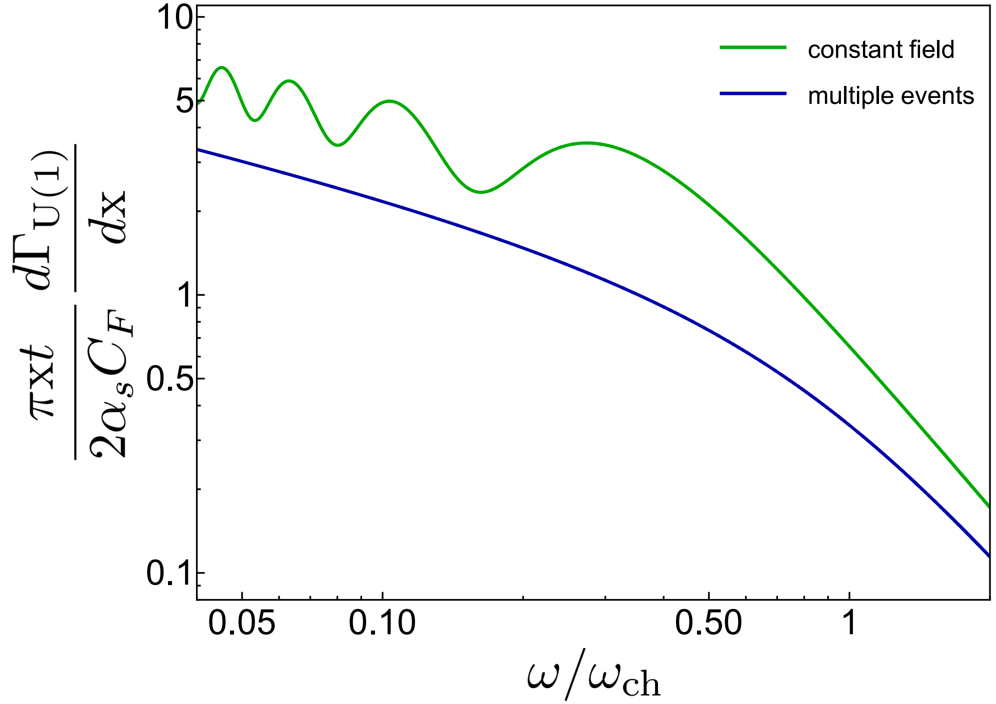

$$\left\langle \frac{d\Gamma_{\rm U(1)}}{d{\rm x}} \right\rangle = \frac{2\alpha_s C_F}{\pi {\rm x}} {\rm Re} \int_0^t \frac{ds}{s^2} \left[\frac{1}{\sqrt{i\frac{E_0^2 s^3}{24\omega}+1}} \left(-1 + \frac{3}{2\left(1 - i\frac{24\omega}{E_0^2 s^3}\right)} \right) + 1 \right]$$

The case of U(1) fields (multiple tubes)

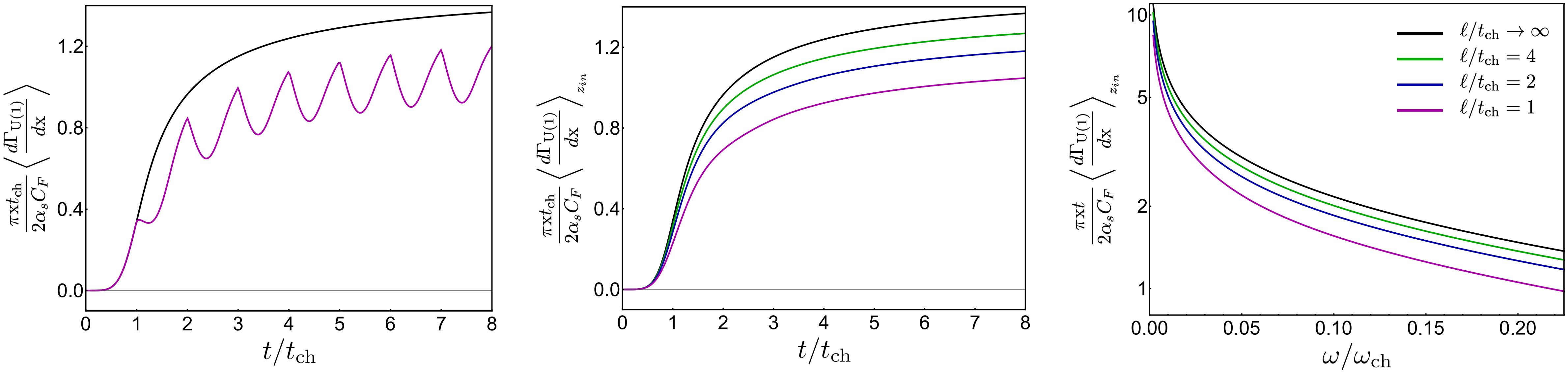

- Notice the destructive interference at the edges and the growth within each tube;
- Upon averaging over the initial position, the series of minima and peaks is smeared -- the rate is similar to the constant field case;
- The greater the number of tubes, the lower the averaged rate (the curves are ordered);

The case of SU(2) fields (multiple tubes)

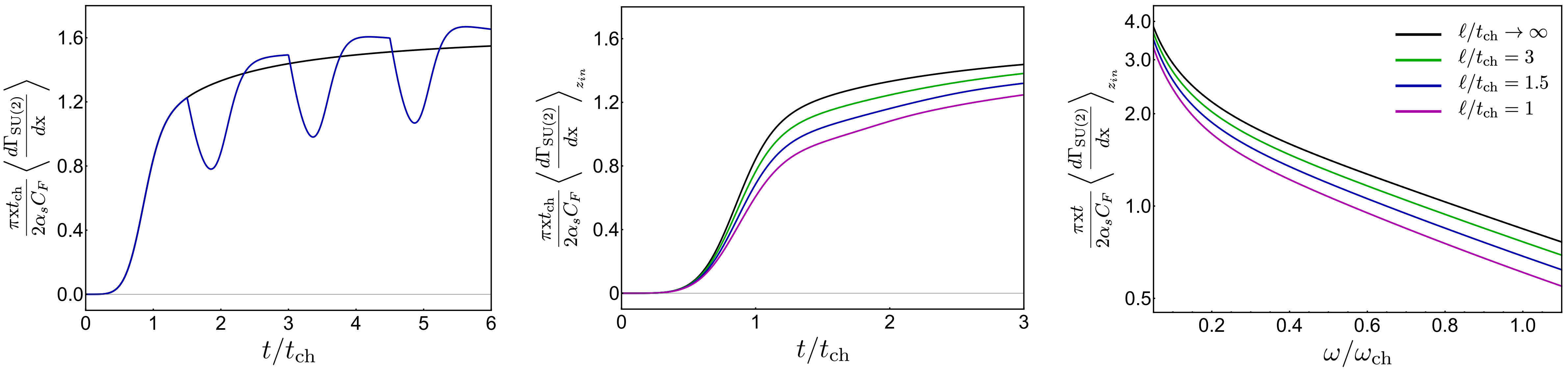

- The same destructive interference pattern with somewhat faster growth;
- Upon averaging over the initial position, the series of minima and peaks is smeared;
- The greater the number of tubes, the lower the averaged rate (the curves are ordered);

The case of U(1) fields

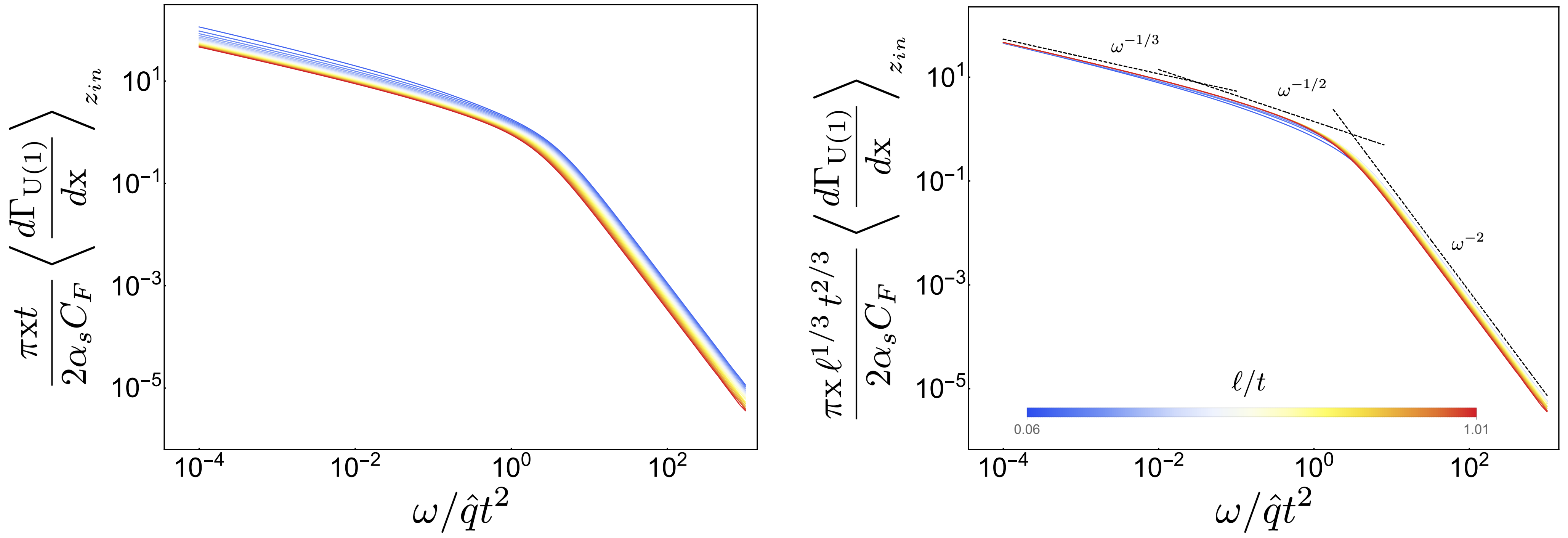

- Sufficiently weak dependence on the tube size at fixed $\hat{q}$;
- The synchrotron-like scaling continues into the region with BDMPS-Z-like behavior;
- Should the harder scatterings be added explicitly?

Summary

- The rate cannot be obtained solely from $\hat{q}$ for a generic profile;
- We have developed a (simple) flexible formalism to describe jet quenching in IS of HIC;
- For the rate we find an intricate interplay of several regimes:
  - When a single flux tube is longer than the formation time (very soft gluons), the rate reproduces the form of synchrotron radiation in a constant field
  - At higher energies, the partons traverse multiple tubes during the emission process, and the rate decreases
  - The rate scales $\omega^{-1/3}$ for lower energies, resembling the constant field case, for the transition region it has a BDMPS-Z like behavior scaling as $\omega^{-1/2}$, and when the formation time is larger than t the rate continues into ω^{-2} tail of the harmonic approximation (lack of harder scatterings)